

MAGNETIC RECONNECTION: RECURSIVE CURRENT SHEET COLLAPSE TRIGGERED BY “IDEAL” TEARING

ANNA TENERANI AND MARCO VELLI
EPSS, UCLA, Los Angeles, CA

ANTONIO FRANCO RAPPAZZO
Advanced Heliophysics, Pasadena, CA

FULVIA PUCCI
Università degli studi di Roma Tor Vergata, Rome, Italy
Draft version November 18, 2018

ABSTRACT

We study, by means of MHD simulations, the onset and evolution of fast reconnection via the “ideal” tearing mode within a collapsing current sheet at high Lundquist numbers ($S \gg 10^4$). We first confirm that as the collapse proceeds, fast reconnection is triggered well before a Sweet-Parker type configuration can form: during the linear stage plasmoids rapidly grow in a few Alfvén times when the predicted “ideal” tearing threshold $S^{-1/3}$ is approached from above; after the linear phase of the initial instability, X-points collapse and reform nonlinearly. We show that these give rise to a hierarchy of tearing events repeating faster and faster on current sheets at ever smaller scales, corresponding to the triggering of “ideal” tearing at the renormalized Lundquist number. In resistive MHD this process should end with the formation of sub-critical ($S \leq 10^4$) Sweet Parker sheets at microscopic scales. We present a simple model describing the nonlinear recursive evolution which explains the timescale of the disruption of the initial sheet.

1. INTRODUCTION

Magnetic reconnection is thought to provide the pathway for energy release in solar flares and other phenomena where energy is accumulated in the magnetic fields and currents of ionized high temperature plasmas. What has remained difficult to understand has been the triggering and speed of the process itself, which, given the extremely large Lundquist (S) and Reynolds (R) numbers, implies that currents must collapse to extremely small scales before anything close to realistic timescales are approached.

Indeed, an active region in the solar corona has a typical spatial scale L of about $L \simeq 10^9$ cm, a magnetic field $B \simeq 50$ G, density $\rho \simeq 10^9$ cm⁻³ and a temperature $T \simeq 10^6$ K, hence a macroscopic Lundquist number $S \simeq 10^{13}$. A flare emits a total energy of about 10^{32} ergs on a typical timescale of a few minutes, which cannot be explained by simple magnetic field diffusion or by a reconnecting instability occurring on the macroscopic scale itself. It has been suggested then that the reconnection trigger might only be provided by kinetic effects, beyond the (resistive) magnetohydrodynamic description of the plasma, or, alternatively, by the fast plasmoid instability of Sweet-Parker current sheets (Cassak & Drake (2013) and references therein).

It has been predicted recently, using linear stability analyses, that the tearing mode instability should grow on ideal timescales (“ideal” tearing, or IT) once the inverse aspect ratio a/L of a current sheet reaches a scale $a/L \sim S^{-1/3}$, preventing the formation of the

paradigmatic Sweet-Parker current sheet (SP) for which $a_{\text{SP}}/L \sim S^{-1/2}$, about 150 times smaller than $S^{-1/3}$ for $S \simeq 10^{13}$ and even smaller for greater S . Even more interestingly, the (linear) asymptotic tearing instability in thin current sheets at arbitrary aspect ratios predicts that the maximum growth rate normalized to the macroscopic Alfvén time increases nonlinearly with the aspect ratio, $\gamma_m \tau_A \sim (L/a)^{3/2}$ (see also eq. (1) below): this suggests that collapse to the critical threshold thickness may provide the trigger for fast reconnection, where “fast” here is meant for dynamics occurring on the ideal timescale (Pucci & Velli 2014; Tenerani et al. 2015; Landi et al. 2015; Del Sarto 2015).

At the intermediate Lundquist numbers usual to simulations, say, $S \simeq 10^4 - 10^5$, the presence of plasma flows into (inflows), and along (outflows) the current sheet affects the scaling of the critical threshold for IT by inducing the formation of more elongated current sheets, that is, of layers having inverse aspect ratios $a/L \sim S^{-\alpha_c}$, with $\alpha_c > 1/3$ (Velli 2015a). Therefore, with the Lundquist number not sufficiently large, the distinction between the IT scaling and the SP scaling might seem academic. Nevertheless, the IT current sheet instability, as typical for the tearing mode, produces a quasi-singular inner layer δ_i , whose inverse aspect ratio follows the SP scaling $\delta_i/L \sim S^{-1/2}$. Such inner layer is however non-stationary, with inflows and outflows increasing exponentially in time—their ratio incidentally does not follow the SP scaling, but rather $u_{\text{in}}/u_{\text{out}} \sim S^{-1/3}$ —together with the amplitude of the reconnecting field: seen from this inner layer, one may interpret the dynamics in terms of the “embedded reconnection” scenario (Cassak & Drake

2009), leading to greater energy storage and more efficient dissipation at the extremely large S values of the solar corona.

Here we study the onset and evolution of the tearing instability within a single collapsing current sheet by means of resistive MHD simulations at $S = 10^6$. In the following paragraphs we first show that the transition to a fast tearing mode instability takes place during the collapse when the predicted threshold inverse aspect ratio $a/L \sim S^{-1/3}$ is reached. Secondly, we show that the secondary current sheets formed nonlinearly give rise to recursive tearing instabilities at increasingly smaller scales and faster super-Alfvénic timescales, which may also be well described by the flow-modified “ideal” tearing criterion and instability. The nonlinear evolution leads to a complete disruption in a timescale estimated at 0.05 percent of the macroscopic Alfvén time once initial tearing is triggered, which we model here in a corrected version of the fractal reconnection scenario first proposed by (Shibata & Tanuma 2001). Though the two-dimensional instability of current sheets and its subsequent nonlinear evolution within resistive MHD has been studied before, it is shown here for the first time that the IT instability scenario, appropriately modified by the effect of the reconnection velocity flows, provides a quantitative description of the various stages in the evolution of a reconnecting current sheet, including hierarchical secondary island formation and disruption. Our results also provide a coherent framework through which previous simulations (Loureiro et al. 2005; Lapenta 2008; Daughton et al. 2009; Battacherjee et al. 2009) may be more completely understood.

2. TRIGGER OF FAST RECONNECTION: SCENARIO

Let us consider a (local) current sheet of inverse aspect ratio a/L , as the one given in eq. (2), with Alfvén speed v_A and magnetic diffusivity η , in a high $S = Lv_A/\eta \gg 1$, constant density plasma. We assume, as in (Uzdensky & Loureiro 2014), that the current sheet is collapsing via some external process on a timescale $\tau_c \sim a(da/dt)^{-1}$, which we take of the order of the ideal timescale, $\tau_c \gtrsim \tau_A = L/v_A$. We extend the linear analysis of the incompressible tearing instability to this time-dependent case by defining an instantaneous growth rate $\gamma(k, t)$, k being the wave number along the sheet, where explicit time-dependence is introduced by the evolving aspect ratio L/a itself.

In the static case, two regimes describe the unstable spectrum of a current sheet: the so called small Δ' regime, for wavelengths close to the instability threshold (or const.- ψ (Furth et al. 1963), for $ka \lesssim 1$ for our equilibrium), and the large Δ' regime (or non const.- ψ (Coppi et al. 1976), for $ka \ll 1$). These two regimes have wave vectors k that lie to the right and to the left of the fastest growing mode k_m , $k_m < k < 1/a$ and $0 < k < k_m$, respectively (Battacherjee et al. 2009; Loureiro et al. 2013; Del Sarto 2015). The wave vector and the growth rate of the fastest growing mode are given by (Pucci & Velli 2014):

$$k_m a \sim S^{-1/4} (L/a)^{1/4}, \quad \gamma_m \tau_A \sim S^{-1/2} (L/a)^{3/2}. \quad (1)$$

Similarly to eqs. (1), the growth rates in the small and large Δ' regimes also increase with the aspect ratio; how-

ever, their values tend to zero in the asymptotic limit $S \rightarrow \infty$, and the full $\gamma(k)$ dispersion relation becomes rapidly peaked around k_m (cfr. Fig. 1 of (Pucci & Velli 2014)). Therefore, both the small and large Δ' regimes can be neglected in the framework of fast reconnection, since the development of the instability is controlled by the evolution of the fastest growing mode described by eqs. (1). Take the current sheet given by eq. (2), for example: the unstable spectrum lies within the range $2\pi/L \lesssim k < 1/a$. From this condition and the first of eqs. (1) it follows that the regime described by eqs. (1) always exists once $k_m L \gtrsim 2\pi$, i.e. once $a/L \lesssim 0.2 S^{-1/5}$. The second of eqs. (1) shows that the growth rate becomes ideal when approaching the critical width $a/L \sim S^{-1/3}$ (much smaller than $S^{-1/5}$) from above: the transition to “ideal” tearing during collapse therefore occurs on the fastest growing mode. In conclusion, a collapse with $\tau_c \gtrsim \tau_A$ naturally drives a sudden switch from a quasi-stable state—growth rate depending on a negative power of S —to an ideally unstable one. Otherwise, the disruption of the current sheet at widths thicker than critical (as considered in (Uzdensky & Loureiro 2014)) would require an infinite time for $S \rightarrow \infty$.

We now consider the example of an exponential collapse. Exponentially thinning current sheets are observed in simulations of solar and stellar coronal heating (Rappazzo & Parker 2013), in 3D MHD turbulence (Brachet et al. 2013; Grauer & Marliani 2000) of interest to a broad range of astrophysical phenomena, as well as in the nonlinear stage of the classic tearing instability itself (Ali et al. 2014).

3. NUMERICAL SET UP

We consider a plasma with homogeneous density ρ_0 and pressure p_0 . The background magnetic field \mathbf{B}_0 describes an exponentially shrinking current sheet and is given by

$$\mathbf{B}_0 = B_0 \tanh[y/a(t)] \hat{\mathbf{x}} + B_0 \operatorname{sech}[y/a(t)] \hat{\mathbf{z}}, \quad (2)$$

where the half width $a(t)$ is prescribed and parametrized in time by

$$a(t) = a_0 \exp^{-t/\tau_c} + a_\infty (1 - \exp^{-t/\tau_c}). \quad (3)$$

We employ a 2.5D compressible MHD code periodic in x and with non-reflecting boundary conditions along the inhomogeneous y direction (Landi et al. 2005). We assume an adiabatic closure, with index $\Gamma = 5/3$, a scalar resistivity, and a Newtonian viscous stress tensor with Prandtl number $P = 1$. With this choice, viscosity does not affect the scalings of IT significantly (Tenerani et al. 2015). The collapse of the background magnetic field is obtained by adding a source term \mathcal{F} of the form

$$\mathcal{F} = \left(\frac{1}{a} \frac{\partial a}{\partial t} \right) y \frac{\partial \mathbf{B}_0}{\partial y} \quad (4)$$

in Faraday’s equation. Magnetic and velocity fields are normalized to B_0 and to $v_A = B_0/\sqrt{4\pi\rho_0}$, respectively, lengths to the macroscopic length L , time to τ_A , and density and pressure to ρ_0 and $B_0^2/4\pi$, respectively. It is useful to introduce also the normalized flux function ψ , such that $\mathbf{B} = \nabla \times \psi \hat{\mathbf{z}}$. We set $p_0 = 0.8$ and $S = 10^6$. Instability is seeded with a random noise of small

Table 1

Simulation parameters: Lundquist number, collapsing time, asymptotic half width, onset time, nonlinear time, and half width reached at the end of the linear stage.

run #	S	τ_c/τ_A	a_∞/L	τ_*/τ_A	τ_{nl}/τ_A	$a(\tau_{nl})/L$
run 1		1	$S^{-1/3}$	3	16	0.01
run 2	10^6	4	$S^{-1/3}$	11.5	22	0.0105
run 3		10	$S^{-1/3}$	16	36	0.013
run 4		1	$S^{-1/2}$	3	4.5	0.0024

amplitude. Because of the wide range of scales to be resolved in the y direction, we employ an inhomogeneous grid with increasing resolution at the neutral line. The simulation box has normalized dimensions $L_x \times L_y = 2\pi \times 0.96$ (runs 1–3) and $L_x \times L_y = 2\pi \times 0.46$ (run 4), with 2048×1024 mesh points. Resolution at the neutral line is $\Delta y = 0.0001$, which allows to resolve the diffusion region of the IT, that scales as $\delta_i/L \sim S^{-1/2}$ (Pucci & Velli 2014). Since for $a \simeq L$ the instability is extremely slow, we start from $a_0 = 0.1 L$. This is a good compromise for limiting computational time while retaining a sufficient dynamical range for the collapse.

4. RESULTS

In Table 1 we list the background and main dynamical parameters for each run, and in Fig. 1 we show for reference the temporal evolution of some unstable Fourier modes of the flux function $\psi_k(y)$, in $y = 0$, from run 2. The growth rate and wave number of the fastest growing mode of the primary tearing at the critical IT threshold will be labelled γ_i and k_i , respectively. In particular, in our simulations we find $k_i L = 10$ and $\gamma_i \tau_A = 0.46$, in agreement with theory (Tenerani et al. 2015).

4.1. Linear stage

Tearing onset takes place at time τ_* such that $\gamma_m(\tau_*)\tau_c = 1$, where $\gamma_m = 0.46 S^{-1/2}(a/L)^{-3/2}$. After onset, the most unstable modes grow according to the WKBJ solution $\psi_m(t) \sim \exp[\int^t \gamma_m(t') dt']$, represented by the dashed line in Fig. 1. In runs 1–3 we consider different cases of collapse in which $a_\infty/L = S^{-1/3}$. In all these runs the linear stage is ultimately dominated by modes

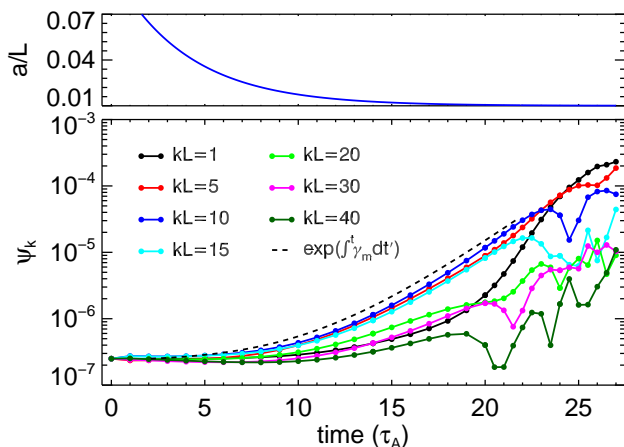


Figure 1. Upper panel: a/L vs. time. Lower panel: temporal evolution of the amplitude of some unstable modes $\psi_k(y)$ at the neutral line $y = 0$ (run 2).

close to the ideally unstable one $k_i L = 10$. Run 4 forces a collapse of the initial sheet down to $a_\infty/L = S^{-1/2}$, but proves that inverse aspect ratios $a/L \ll S^{-1/3}$ cannot be formed: the tearing mode indeed ignites right after $t = 2.4 \tau_A$, at which $a/L = S^{-1/3}$, and a large number of islands rapidly pop up. Even at the end of the linear stage (see Section 4.2) the collapsing sheet thickness is twice the corresponding SP thickness at the given S and P (Tenerani et al. 2015).

4.2. Early nonlinear stage

Nonlinearity becomes important at τ_{nl} , when the width w of magnetic islands is of the order of the width of the inner diffusion layer δ . The fastest growing mode has δ_m which scales with the aspect ratio as $\delta_m/a \sim (av_A/\eta)^{-1/4}$ (Loureiro et al. 2013), hence $\delta_m/a \sim S^{-1/4}(L/a)^{1/4}$. By using the definition $w/a \simeq 2\sqrt{\psi_m/a}$ (Biskamp 2000), we estimate the amplitude $\psi_m(\tau_{nl}) \simeq 0.25 S^{-1/2} [a(\tau_{nl})/L]^{1/2} \simeq 2.5 \times 10^{-5}$, in agreement with simulations. Nonlinear effects lead to the competition of two processes (Malara et al. 1991): on the one hand, islands start to merge through an inverse cascade process from the fastest growing modes to smaller wave numbers, see, e.g., the inverse cascade from $k_i L = 10$ towards $kL = 5$ and below starting at $\tau_{nl} = 22 \tau_A$ (Fig. 1); on the other hand, X-point collapse, and subsequent secondary current sheet formation, takes place during the further nonlinear growth of the islands, as is typical for strongly unstable modes far from the small Δ' regime (Jemella et al. 2003), in lieu of the slow, algebraic Rutherford growth (Rutherford 1973).

4.3. Nonlinear stage: recursive X-point collapse

We analyze the fully nonlinear stage using run 1 as a reference, shown in Fig. 2. X-point collapse proceeds leading to the formation of secondary plasmoids (magnetic islands) (Loureiro et al. 2005; Lapenta 2008) and, next, a recursive process of super-Alfvénic secondary layer formation and disruption, takes place (Shibata & Tanuma 2001; Daughton et al. 2009; Battacharjee et al. 2009). Fig. 2 shows a temporal sequence of recursive plasmoid formation, taking place at the center, near the flow stagnation point of the original instability. Previously, such recursive reconnection has been modeled as a succession of unstable SP layers (Loureiro et al. 2005; Daughton et al. 2009; Cassak & Drake 2009; Huang & Battacharjee 2010; Uzdensky et al. 2010; Loureiro et al. 2012). Our simulations show instead that it is driven by onset of the IT mode, triggered by the dynamical *lengthening* of sheets to the local critical threshold, in a way similar to that discussed in section 4.1. As the recursive X-point collapse occurs in steps, we label the half length of the n -th current sheet L_n , the inverse aspect ratio a_n/L_n , the normalized (half) width of the inner diffusion layer δ_n/L_n , the local Lundquist number $S_n = (L_n/L)S$ and Alfvén time $\tau_{A,n} = (L_n/L)\tau_A$. Referring to Fig. 2, the recursive X-point collapse starts with the formation of L_1 from the primary diffusion region of thickness δ_i , hence $a_1 \simeq \delta_i$. Current sheet L_1 becomes unstable, less than $3 \tau_A$ after the end of the linear stage (second panel), consistent with what was found in (Landi et al. 2015). Here we

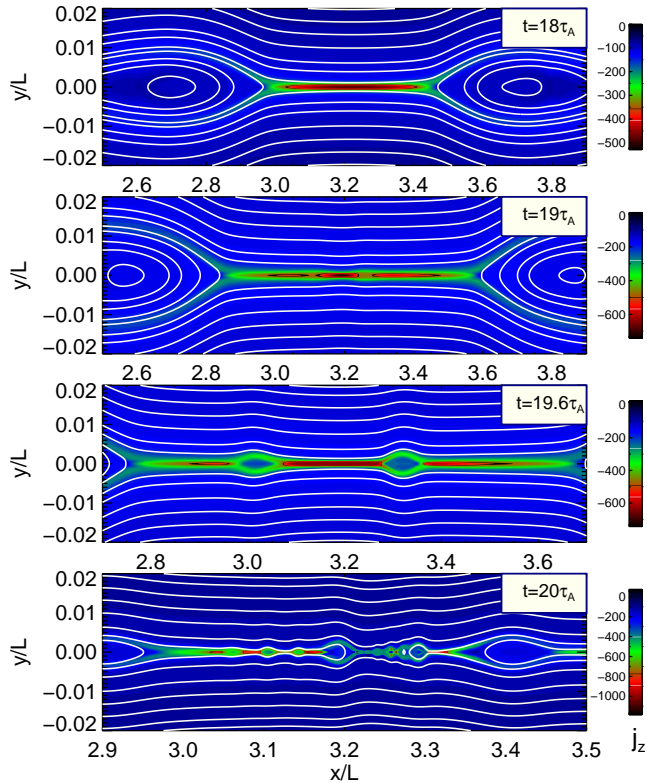


Figure 2. Blow-up of the recursive “ideal” tearing instability in run 1: contour plot of the out-of-plane current density j_z (color coded) and magnetic field lines (white). Notice that the whole domain is much larger, $0 \leq x/L < 2\pi$ and $-0.48 \leq y/L \leq 0.48$.

show that IT triggering within L_1 induces the growth of two plasmoids and of a second current L_2 , with $a_2 \simeq \delta_1$ (third panel), which is itself destroyed by multiple plasmoids in about $0.5 \tau_A$ (fourth panel). In Fig. 3 we plot $B_y(y, x_0)$, in $x_0/L = 3.2$, at three different times. The shown profiles of the magnetic field closely resemble the tearing mode eigenfunction, and display a clear hierarchical structure within each of the inner diffusion layers. To further analyze the tearing onset inside such secondary layers, in Fig. 4 we display L_1/L (in green), a_1/L (ma-

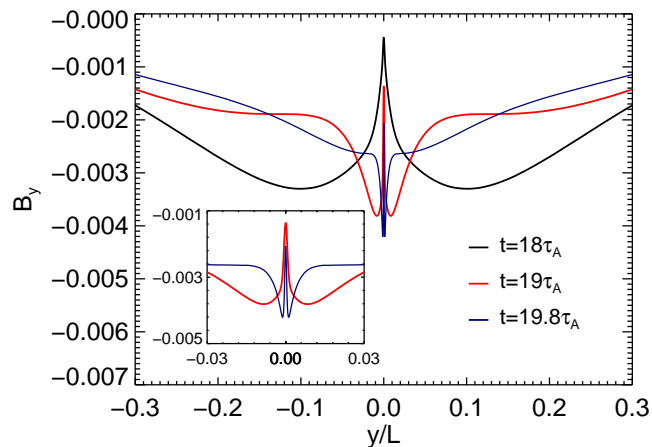


Figure 3. Profile of $B_y(y, x_0)$ in $x_0/L = 3.2$ at $t = 18 \tau_A$ (primary tearing, $n = 0$), $t = 19 \tau_A$ ($n = 1$), and $t = 19.8 \tau_A$ ($n = 2$). The inset is a blow-up of $B_y(y, x_0)$ at $t = 19 \tau_A$ and $t = 19.8 \tau_A$.

genta), and a_1/L_1 (in blue) as a function of time, from $t = 15 \tau_A$, up to $t = 19 \tau_A$. During the collapse process the width remains almost constant, $a_1 \simeq \delta_i \sim LS^{-1/2}$ (here $\delta_i \simeq 0.0015$), while the length L_1 stretches at about a rate $\dot{L}_1/L_1 \simeq 1/\tau_{c,1}$, $\tau_{c,1} \simeq 2\tau_A$. Fig. 4 shows that a_1/L_1 crosses the critical threshold $S_1^{-1/3}$ (red dotted line) at $t \simeq 16 \tau_A$. At that time $L_1 \simeq 0.1 L$, thus $S_1 \simeq 10^5$, $P = 1$, and linear theory predicts $\gamma_{i,1}\tau_{A,1} \simeq 0.47$, or $\gamma_{i,1}\tau_A \simeq 2.3 \gg \tau_{c,1}^{-1}\tau_A$. In the light of the previous discussion, we would expect L_1 to disrupt more rapidly than in $\simeq 3 \tau_A$, though on the same order of magnitude timescale. On the other hand, there is a stabilizing effect from outflows forming along L_1 (Bulanov et al. 1978): these may induce the formation of thinner sheets having inverse aspect ratio $a_n/L_n \sim S_n^{-\alpha_c}$, with $\alpha_c > 1/3$. Based on the empirical observation that flows stabilize SP up to $S_c \simeq 10^4$, one can extend the IT theory to find a critical α_c which includes the effect of inflow-outflows (Velli 2015a):

$$\alpha_c = \frac{2 \log \mu + \log S_n}{3 \log S_n}. \quad (5)$$

In eq. (5), $\mu = \Gamma_v/(f\gamma_i)$ is the ratio of the plasmoid evacuation rate to the maximum growth rate, corrected by a threshold factor $f \simeq 0.5 - 0.1$. The value $\mu = 10$ (Biskamp 2000) yields the observed $\alpha_c = 1/2$ for $S_n = 10^4$, while as expected $\lim_{S_n \rightarrow \infty} \alpha_c = 1/3$. Note that,

as shown below, S_n is a decreasing function of n . The black dotted and dash-dotted lines in Fig. 4, correspond to $S_1^{-\alpha_c}$ at two different μ , while the light blue dotted line corresponds to $a_{SP,1}/L_1$. Though our Lundquist numbers are not extremely large, L_1 still disrupts before reaching the SP width. The trend of the data plotted in Fig. 4 goes in the direction of our scenario, that is, that the fast tearing instability is triggered within collapsing current sheets once the critical threshold is reached. Taking into account the increased Alfvén speed due to pile-up just outside the inner diffusion region as considered by (Cassak & Drake 2009) does not change the trend of our results. Interestingly, the discussion of flux pile-up and embedded reconnection led (Cassak & Drake 2009) to independently find a similar scaling $\sim S^{-1/3}$ for the inverse aspect ratio of unstable current sheets starting from an initial secondary Sweet-Parker sheet. Their analysis starts from a different line of thought, in the search for the proper criterion to destabilize an embedded SP sheet, and proceeds via a linearization of the fields in the neighborhood of the neutral line. It then finds a scaling with S for the aspect ratio of the embedded layer scaling in a way similar to IT. On the other hand, the IT scaling derives from requiring an S -independent growth rate from the complete eigenmode analysis of tearing instability theory, and finds that the entire sheet inverse aspect ratio scales as $S^{-1/3}$. The results therefore have different origin, and for the IT case the presence of flows modifies the scaling exponent α_c according to eq. (5): incidentally, the latter expression is in excellent agreement with the aspect ratios at which plasmoids are observed to be ejected in the (Cassak & Drake 2009) paper.

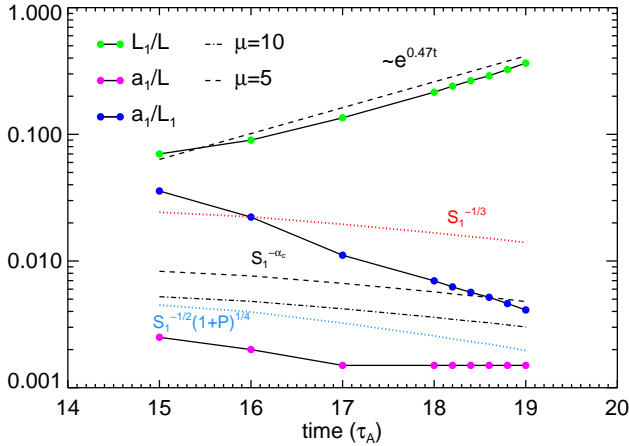


Figure 4. Length L_1/L (green), width a_1/L (magenta), and inverse aspect ratio a_1/L_1 (blue) of the first secondary current sheet vs. time (run 1). The red dotted line represents the critical threshold $S^{-1/3}$, and the light blue dotted line the viscous a_{sp}/L . Black dotted and dash-dotted lines represent the critical threshold with outflow effects, given by eq. (5).

We have shown that a collapsing current sheet disrupts due to the triggering of fast reconnection as predicted by the IT model. This process is shown to proceed recursively, giving rise to a hierarchy of fast tearing instabilities at ever smaller scales. Let us model the recursive collapse of X-points, in the spirit of the original fractal reconnection model, with the following differences: first, we don't consider SP as the initial condition; second, we use the width a_n , derived from the IT scalings, to find L_n . Neglecting for simplicity viscous and outflow effects, imposing that $a_n/L_{n-1} \sim S_{n-1}^{-1/2}$ (i.e., $a_n \simeq \delta_{n-1}$), and that IT onset occurs at $a_n/L_n \sim S_n^{-1/3}$, we find:

$$L_n = L S^{-1+(3/4)^n}, \quad \tau_{A,n} = L_n \tau_A, \quad S_n = S^{(3/4)^n}. \quad (6)$$

For $n \rightarrow \infty$ then $\tau_{A,n} \rightarrow \tau_A S^{-1}$, and, as expected, $S_n \rightarrow 1$ and $a_n/L_n \rightarrow 1$. However, after a number n_* of steps $S_{n_*} \simeq 10^4$, at which we expect to reach a stable SP. For $S = 10^{13}$ (solar corona) $n_* \simeq 4$, and the length L_n suddenly drops to microscopic scales, $L_1/L \simeq 6 \times 10^{-4}$, $L_2/L \simeq 2 \times 10^{-6}$, $L_3/L \simeq 3 \times 10^{-8}$, $L_4/L \simeq 10^{-9}$. The recursive X-point collapse after the first trigger thus lasts a time interval $\tau_{tot} \simeq \sum_{n=1}^{n_*} \tau_{A,n} \simeq 5 \times 10^{-4} \tau_A$, one order of magnitude less than the upper limit given by (Shibata & Tanuma 2001). Higher resolution simulations are nevertheless necessary to assess how the non-linear evolution saturates. Our scenario can be modified to include kinetic scales which might be reached dynamically in typical astrophysical systems (Cassak et al.

2005; Daughton et al. 2009). In this case we expect a change of the power laws (6) as different scalings describe the physics at the critical threshold in the kinetic regime (Del Sarto 2015).

We thank D. Del Sarto for interesting discussions and useful comments. This work was supported by NASA via the Solar Probe Plus Observatory Scientist grant.

REFERENCES

- Ali, A., Jiquan Li & Kishimoto Y. 2014, 21, 052312
 Bhattacharjee, A., Huang, Yi-Min, Yang, H. & Rogers, B. 2009, Phys. of Plasmas, 16, 112102.
 Biskamp, D., 2000, Magnetic Reconnection in Plasmas (Cambridge University Press, England)
 Brachet, M., Bustamante, M. D., Krstulovic, G., Mininni, P. D., Pouquet, A., and Rosenberg, D. 2013, PhRvE, 87, 131110
 Bulanov, S. V., Syrovatskii, S. I., & Sakai, J. 1978, JETP 28, 177
 Cassak, P. A., Shay, M. A., & Drake, J. F. 2005 Phys. Rev. Lett., 95 235002
 Cassak, P. A., & Drake, J. F. 2009, ApJ 707, L158
 Cassak, P. A. & Drake, J. F. 2013, Phys. Plasmas 20, 061207
 Coppi, B., Pellat, R., Rosenbluth, M., & Galvao, R. 1976, Soviet Journal of Plasma Physics, 2, 533
 Daughton, W., Roytershteyn, V., Albright, B. J., Karimabadi, H., et al. 2009, Phys. Rev. Lett. 103, 0065004
 Del Sarto, D., 2015, private communication
 Furth, H. P., Killeen, J., & Rosenbluth, M. N. 1963, Phys. Fluids 20, 459
 Grauer, R. & Marliani, C. 2000, PRL, 84, 4850
 Huang, Yi-Min, Bhattacharjee, A. 2010, Phys. of Plasmas, 17, 062104
 Jemella, B. D., Shay, M. A., & Drake, J. F., 2003, Phys. Rev. Lett. 91, 125002
 Landi, S., Velli, M., & Einaudi, L. 2005, ApJ 624, 392
 Landi, S., Del Zanna, L., Papini, E., Pucci, F., et al. 2015, 806, 131
 Lapenta, G. 2008, Phys. Rev. Lett. 100, 235001
 Loureiro, N. F., Cowley, S. C., Dorland, W. D., Haines, M. G., et al. 2005, Phys. Rev. Lett. 95, 235003
 Loureiro, N. F., Schekochihin, A. A., & Cowley, S. C. 2007, Phys. Plasmas, 14, 0703
 Loureiro, N. F., Samtaney, R., Schekochihin, A. A., & Uzdensky, D. A. 2012, Phys. Plasmas, 19, 042303
 Loureiro, N. F., Schekochihin, A. A., & Uzdensky, D. A. 2013, Phys. Rev. E 879, 013102
 Malara, F., Veltri, P., & Carbone, V. 1991, Phys. Fluids B 3, 1801
 Pucci, F. & Velli, M. 2014, ApJL, 780, L19
 Rappazzo, A.F., & Parker, E. N. 2013, ApJL, 773, L2
 Rutherford, P. H. 1973, Phys. Fluids 16, 1903
 Samtaney, R., Loureiro, N. F., Uzdensky, D. A., Schekochihin, A. A. et al. 2009, Phys. Rev. Lett. 103, 105004
 Shibata, K., & Tanuma, S. 2001, Earth Planets Space 53 473
 Tenerani, A., Rappazzo, A. F., Velli M., & Pucci, F. 2015, ApJ 801, 145
 Uzdensky, D. A., Loureiro, N. F., & Schekochihin, A. A. 2010, Phys.Rev. Lett. 105 235002
 Uzdensky, D. A., & Loureiro, N. F. 2014, arXiv:1411.4295
 Velli, M., 2015a, private communication
 Velli, M., Pucci, F., Rappazzo, A. F., & Tenerani, A., 2015b, Phil. Trans. R. Soc. A 373, 20140262